Dynamic simulation of steam generation system in solar tower power plant

Qiang Zhang[1], Zhiming Wang[1], Xiaoze Du[2,1†], Gang Yu[1], Hongwei Wu[3]

1 Key Laboratory of Condition Monitoring and Control for Power Plant Equipment (North China Electric Power University), Ministry of Education, Beijing 102206, China

2 School of Energy and Power Engineering, Lanzhou University of Technology, Lanzhou 730050, China

3 School of Engineering and Computer Science, University of Hertfordshire, Hatfield, AL10 9AB, UK

Abstract

Concentrated solar power plant (CSP) with thermal energy storage can be operated as peak load shaving plant, which is one of the most economic solutions to the intermittency of renewable energy grid. The steam generation system (SGS) is the central hub between the heat transfer fluid and the working fluid of CSP, of which the dynamic characteristics need to be further investigated. The SGS of Solar Two power tower plant with the molten salt as both the heat transfer fluid and storage media is selected as the object. The mathematical model with lumped parameter method is developed to analyze its dynamic characteristics. Model validation is carried out and it shows that the proposed model can simulate the characteristics of SGS in an accurate manner. Five simulation tests were carried out under the disturbances that the molten salt solar tower power plant may encounter under various solar irradiation and output electrical load. Both the dynamic and static

† Corresponding author. Tel.: +86(10)61773923; Fax: +86(10)61773877. Email address: duxz@ncepu.edu.cn (X. Du)

characteristics of SGS are analyzed with the response curves of the system state parameters obtained under different disturbances. The dynamic response and time constants of the working fluids out of the SGS is obtained when step disturbances is imposed. It is indicated that the disturbances imposed to both working fluids lead to heat load reassignment to the preheater, evaporator and superheater. The proposed step-by-step disturbance method can reduce the fluid temperature and pressure fluctuations by 1.5 °C and 0.03 MPa, respectively. The results obtained could be used as the references for control strategies as well as the safe operation of and SGS.

Keywords: concentrated solar power tower, molten salt, steam generation system, dynamic simulation

Nomenclature

A area, m^2

c_p specific heat capacity at constant pressure, kJ/kg·°C

Flow mass flow rate (calculation result), kg/s

h enthalpy, kJ/kg

k_d resistance coefficient of the tube bundle

$\dot{m}$ mass flow rate, kg/s

Nu the Nusselt number

P_d continuous discharging rate (%)

P pressure, MPa

Pr the Prandtl number

Q heat flux, kW

r latent heat of water, kJ/kg

T temperature, °C

U surfaceheat transfer coefficient, kW/(m^2·°C)

V volume of the shell for evaporator and volume of the tube side for the preheater and superheater, m^3

X quality, kg

Greek symbols

ξ linear admittance

λ thermal conductivity, W/(m·°C)

μ dynamic viscosity, Pa·s

Subscripts

e evaporator

evap evaporation

f feedwater

i inlet

o outlet

p preheater

s molten salt or superheater

t tube

v steam/vapor

w water

1. Introduction

Nowadays, the continuous decreasing cost of the wind turbine and photovoltaic (PV) panels, as well as the challenges of global environmental problems, are driving rapid deployment of the renewable energy around the world. For example, in China, it is expected that the installed wind power capacity will exceed 200 GW, and the installed PV power capacity will exceed 242 GW by 2020 [1], while the renewable electricity will have a proportion of 27% on national electricity demand [2].

It is recognized that the intermittency and uncertainty of wind energy and solar energy present a significant challenge to their power output, which will affect the stability of the grid and lead to serious power curtailment. Therefore, electrical power sources which are flexible are required to be functioned as peaking plants [3]. Energy storage could be an option to improve the flexibility of power grid with high proportion of renewable energy by shifting power output to the periods of high demand. By the end of 2016, China has 24.3 GW operational capacity of energy storage, including pumped hydroelectric energy storage (98.96%), electrochemical storage (1%) and thermal energy storage (0.04%) [2]. Considering that the hydroelectric could have its future barrier, there is a tremendous opportunity to develop high energy density and cost-effective energy storage technology.

The simplistic approach to determine a generation technology might be based on the option with the lowest overall levelized cost of electricity (LCOE) and capital cost. Several electrochemical storages of battery technologies have an LCOE over 20 ¢/kWh [4,5]with approximately 300 $/kW in capital cost. Compare to the expensive battery technology, the cost of thermal energy storage

(TES) can be below to 20-25 \$/kWh [6,7]. Moreover, TES can reduce the cost of the concentrating solar power (CSP) by around 10% [8,9].

Among all the CSP technologies, PT can achieve higher-temperature operation compared to other CSP technologies and yield higher thermal-to-electric conversion efficiency [10, 11]. The two types of PT are differentiated by water/steam or molten salt heat-transfer fluid in the receiver. In a steam-direct PT, steam heated in the receiver directly can achieve a temperature over 550 °C, which is a little higher than the steam temperature (540°C) in a molten-salt PT. Whereas the thermal energy storage capability is higher in a molten-salt PT, with which the PT can be decoupled from electricity generation [11,12], endows the solar tower power plant the load peak shaving capacity.

The net load ramp rate of PT with TES, which operates as a peaking plant, must vary rapidly in a high renewable electricity scenario [8,13]. The dynamic characteristics concern to the operation safety of PT need to be investigated, including the dynamic performances of PT receiver, steam generator, thermal storage system, and steam turbine [14-16]. To better understand the dynamic performances of the steam generator in PT, which act as a peaking plant in the multi-energy integration system to carry out peak-valley regulation, will be especially significant. It is noticed that during the starting, shutting down and varying working conditions of PT, the steam generator will suffer strong thermal stress [17-20]. In order to make continuous improvements in PT safety, reliability, and efficiency, it is necessary to analyze the limitation of the rate of temperature variation. Thus, the dynamic characteristics of PT, especially the steam generator which is the hinge of steam generation system and salt system need to be studied in detail [21].

There are two kinds of simulating models proposed for the shell-and-tube heat exchangers. One is three-dimensional numerical model with high spatial resolution, such as the finite volume method

[22]. The other is the analytical model with low spatial resolution, such as the LPM [8,23,24]. In order to improve the economic performance and optimize the heat exchanger design, a three-dimensional model is applied [25-27]. On the other hand, for transient response simulations, the model with lower spatial resolution is chosen to evaluate the heat exchanger operation and control strategies.

Till now, most of researches have been devoted to study the dynamic characteristic of the solar thermal power plant. The steam-direct DAHAN tower power plant was modeled by Xu [28,29], of which the dynamic characteristics were discussed. Besides, the dynamic simulation of an indirect thermal storage tank was carried out by Li and Xu [8]. Due to the great similarities between the steam-direct solar tower power plant and the conventional thermal power plant, most of the previous studies concerning the dynamic simulations of the solar power plant were focused on steam-direct solar tower power plant. The former studies mainly focused on the impact of radiation on a stand-alone PT, which means only mass flow rate disturbance of the working fluid to SGS is studied. Molten salt PT is more widely used for its potential of energy storage. There are seldom works on the molten-salt solar power tower plant, which will have great potential as the peaking plant in the grid with high proportion of renewable energy for its flexibility when it is cooperated with TES. The structures of the heat exchanger between SGS of a steam-direct PT and a molten salt PT are different. In a steam-direct PT, only water flows through SGS, which is heated by radiation directly. The SGS of a steam-direct PT is very similar to the boiler of a conventional power plant. The temperature of working fluid in a steam-direct PT is high. Only water/steam side could be controlled during operation. In a molten salt PT, water is not exposed to radiation, but heated by molten salt in the heat exchangers. Both working fluid and heat transfer fluid could be well controlled, which means more factors could have influence on the performance of SGS.

Therefore, a mathematical model is built in the current study based on the steam generation system (SGS) of Solar Two molten-salt solar power-tower plant established by Sandia, which includes a preheater, an evaporator and a superheater. These heat exchangers are shell and tube heat exchanger, and the shell of the evaporator is kettle type [20].

In this study, a mathematical model using LPM is developed to study the transient response of a Solar Two SGS under different disturbances. The dynamic model could be a general model for a PT. The aim of the current work is to mainly discuss the process of disturbance influence on SGS, as well as the dynamic behavior resulted from the disturbances and different characteristic time of system responds. This would be the basis to obtain the control strategy during SGS operation. Five disturbance factors which a netconnected PT may encounter are imposed to the SGS. Model response curves of SGS is obtained under five different disturbances. Both the dynamic and static characteristics of SGS are analyzed in detail based on the model response curves of the system parameters that are obtained from different disturbances. A step-by-step adjusting method on the basis of time constant is proposed to decrease the pressure and temperature fluctuation in SGS under different working conditions. Conclusions of this paper could be used to provide references for control strategies including the descision making of the minimum stable load, net load ramp rate of PT as a peaking plant in a multi-energy system.

2. Modeling on the steam generation system

2.1 Physical model

A typical steam generation system of a PT consists of a preheater, an evaporator, a superheater and a reheater. However, the 10MW Solar Two does not have a reheater for the refurbished turbine, same as the non-reheat Solar One. The schematic diagram is shown in Fig. 1. Both the preheater and superheater are made of U-tube, straight-shell. The high pressurized water is placed on the tube side in order to achieve low manufacture cost. The molten salt instead of the high pressurized steam is placed on the shell side so that material is saved becaused of the thinner shell wall[30].

Water flows through the shell of the kettle evaporator reversely, and molten salt flow through the tube crossly. Feedwater is pumped into the preheater with a temperature of 260 °C and pressure of 10.4MPa, and then heated by preheater to the outlet temperature of around 310 °C, which approaches the saturated temperature. The process of vaporization that feed water turns into high-quality saturated steam takes place in the evaporator. The superheater produces superheated steam at approximately 535 °C, then it was attemperated with feed water to meet the temperature requirement of the turbine inlet. The molten salt enters SGS at 565 °C and is cooled to 290 °C.

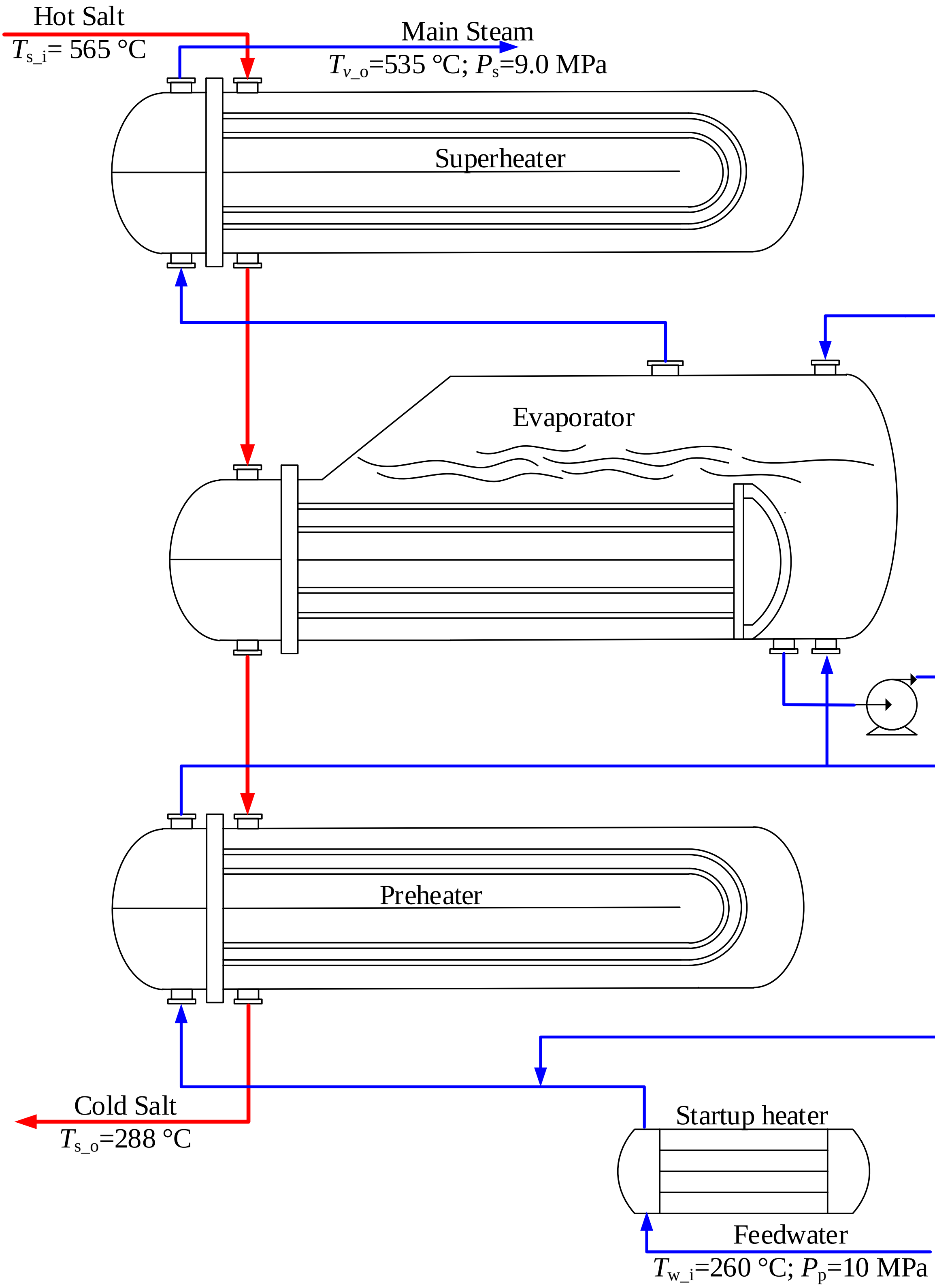

Fig. 1. The schemetic diagram of SGS**.**

The molten salt used in Solar Two is the solar salt consist of 60% $NaNO_3$ and 40% KNO_3. The material selection is different for the three heat exchanger because of the corrosion and operation temperature considerations. S304 stainless steel is used when the operating temperature is over 454 °C, whereas the low carbon steel is used to lower the cost when the operating temperature is below 400 °C. The evaporator tube is made of 2 ¼Cr-1 Mo alloy steel and the shell is made of carbon steel since its operating temperature will not surpass 454 °C[31]. The detailed physical size of SGS is listed in Table1.

Table 1. Geometrical and physical parameters of SGS.

Parameters	**Preheater**	**Evaporator**	**Superheater**
Heat exchange area/m^2	76.2	158.4	152.4
Designed surface heat transfer coefficient at rated conditions/$W/m^2\cdot°C$	1940	1392	911
Tube type	U-type/water	U-type/salt	U-type/steam
Inner diameter/mm	143	135	143
Outer diameter/mm	203	192	203
Design pressure/MPa	10.5	10	10
Operating pressure at rated conditions/MPa	10.4	9.8	9.0
Rated thermal load/MW	3.79	19.82	11

The functions of molten salt physical properties used in this study are listed in table 2.

Table 2. The physical properties of the molten salt.

Property	Function
Density, kg/m^3	$\rho = 2090 - 0.636 \times T$
Specific heat, J/kg. °C	$c_p = 1443 + 0.172 \times T$
Thermal conductivity, W/(m.°C)	$\lambda = 0.443 + 1.9 \times 10^{-4} \times T$
Dynamic viscosity, Pa.s	$\mu = \left(22.714 - 0.120 \times T + 2.281 \times 10^{-4} \times T^2 - 1.474 \times 10^{-7} \times T^3\right) \times 10^{-3}$
Enthalpy, J/kg	$h_s = \int_{270\ °C}^{T_s} c_{p\_s} dT$

2.2 Mathematical model

Considering that the dynamic model of SGS is on system level which includes a preheater, an evaporator and a superheater, the finite volume method (FVM) will not be the best option in this case due to its complexity. In the current work, LPM will be selected to establish the model and Runge-Kuta method is used to solve the differential equations.

In the model, a typical point is chosen to represent the tube side and shell side, respectively. Arithmetic mean value which represent the inlet parameter and outlet parameter and the outlet parameter are used as the typical points of the heat exchangers. The former is picked for the convenience of calculation which could depict the general state of fluid in the heat exchanger. The latter is picked to describe the fluids parameter variation results. However, the nature weakness of the LPM should be noted. The LPM couldn’t display the parameter variation along the tubes which FVM could carry out. But the accuracy the LPM provided is good enough for the study. During the simulation of the model, the time step is 0.01s which remains constant. The simulation doesn’t include the startup and closing down procedure. Disturbances happened when the system is working at a certain condition.

The following assumptions and simplifications are implemented when the steam generation system is modeled.

(1) The axial and circumferential heat conduction of the working fluid and metal wall is ignored.

(2) During the operation, the volume flow rate variation caused by the working fluid density is ignored, for the density changes with the temperature during operation is small.

(4) Water flows out of the preheater is single phase, when it flows into the evaporator, a small part of saturated steam is generated immediately, the rest will be heated by solar salt in the tube.

(5) Steam at the evaporation zone can be regarded as saturated steam. In general, lumped parameter at each section is represented by the outlet parameter or arithmetic mean value.

(6) The temperature of the metal wall is represented by the mean temperature of the inner wall and outer wall.

In addition, all the surface heat transfer coefficients of the three heat exchangers are calculated using the functions provided by the solar power tower design basis document [30]

The governing equations of mass, momentum and energy conservations are stated as follows.

(1) Evaporator

The energy balance in the tube bundle,

$$\frac{\mathrm{d}\left(c_{\mathrm{p\_s}} X_{\mathrm{s}} T_{\mathrm{s}}\right)}{\mathrm{d}t} = \dot{m}_{\mathrm{s}} \left(h_{\mathrm{s\_i}} - h_{\mathrm{s\_o}}\right) - Q_{\mathrm{s}} \qquad (1a)$$

Because of the density change of molten salt during operation is little, the change of X_s with time is ignored, so Eq. (1a) can be simplified as,

$$\frac{\mathrm{d}T_\mathrm{s}}{\mathrm{d}t}=\frac{\dot{m}_\mathrm{s}\left(h_\mathrm{s\_i}-h_\mathrm{s\_o}\right)-Q_\mathrm{s}-\dfrac{T_\mathrm{s}X_\mathrm{s}\mathrm{d}c_\mathrm{p\_s}}{\mathrm{d}t}}{c_\mathrm{p\_s}X_\mathrm{s}} \tag{1b}$$

The specific heat change of molten salt during operation is small, Eq. (1b) can be simplified as,

$$\frac{\mathrm{d}T_\mathrm{s}}{\mathrm{d}t}=\frac{\dot{m}_\mathrm{s}\left(h_\mathrm{s\_i}-h_\mathrm{s\_o}\right)-Q_\mathrm{s}}{c_\mathrm{p\_s}X_\mathrm{s}} \tag{1c}$$

The heat transfer from solar salt to the tube bundle,

$$Q_\mathrm{s}=U_\mathrm{i}A_\mathrm{i}\left(T_\mathrm{s}-T_\mathrm{t}\right) \tag{2}$$

The heat transfer from tube bundle to water and steam**,**

$$Q_\mathrm{w}=U_\mathrm{o}A_\mathrm{o}\left(T_\mathrm{t}-T_\mathrm{w}\right) \tag{3}$$

The energy balance at the tube,

$$\frac{\mathrm{d}\left(c_\mathrm{p\_t}X_\mathrm{t}T_\mathrm{t}\right)}{\mathrm{d}t}=Q_\mathrm{s}-Q_\mathrm{w} \tag{4}$$

in which, $c_\mathrm{p\_t}$=0.499 kJ/kg·°C.

The mass balance on water side,

$$\frac{\mathrm{d}X_w}{\mathrm{d}t}=\dot{m}_\mathrm{f}+\dot{m}_\mathrm{cond}-\dot{m}_\mathrm{evap}-\dot{m}_\mathrm{d} \tag{5}$$

The mass balance on steam side,

$$\frac{\mathrm{d}X_\mathrm{v}}{\mathrm{d}t}=\dot{m}_\mathrm{evap}-\dot{m}_\mathrm{cond}-\dot{m}_\mathrm{v\_o} \tag{6}$$

The mass balance on shell side,

$$\dot{m}_\mathrm{f}-\dot{m}_\mathrm{v\_o}=\frac{\mathrm{d}(V_\mathrm{v}\rho_\mathrm{v}+V_\mathrm{w}\rho_\mathrm{w})}{\mathrm{d}t} \tag{7}$$

The energy balance on shell side,

$$Q_\mathrm{w}+\dot{m}_\mathrm{f}h_\mathrm{f}-\dot{m}_\mathrm{v\_o}h_\mathrm{v}=\frac{\mathrm{d}(V_\mathrm{w}\rho_\mathrm{w}h_\mathrm{w}+V_\mathrm{v}\rho_\mathrm{v}h_\mathrm{v}+X_\mathrm{t}c_\mathrm{p\_t}T_\mathrm{t})}{\mathrm{d}t} \tag{8}$$

In Eqs. (7) and (8), $V_\mathrm{w}+V_\mathrm{v}=V$=constant, $\mathrm{d}/\mathrm{d}t=\partial/\partial P(\mathrm{d}P/\mathrm{d}t)$, $h_\mathrm{w}+r=h_\mathrm{v}$, then,

$$\frac{\mathrm{d}P}{\mathrm{d}t}=\frac{Q_{\mathrm{w}}+\left(\frac{r\rho_{\mathrm{v}}}{\rho_{\mathrm{w}}-\rho_{\mathrm{v}}}-H_{\mathrm{f}}\right)\dot{m}_{\mathrm{f}}-\left(\frac{r\rho_{\mathrm{w}}}{\rho_{\mathrm{w}}-\rho_{\mathrm{v}}}\right)\dot{m}_{\mathrm{v\_o}}}{\left[\rho_{\mathrm{w}}\frac{\partial H_{\mathrm{w}}}{\partial P}+\frac{r\rho_{\mathrm{v}}}{\rho_{\mathrm{w}}-\rho_{\mathrm{v}}}\left(\frac{\partial\rho_{\mathrm{w}}}{\partial P}\right)\right]V_{\mathrm{w}}+\left[\rho_{\mathrm{v}}\frac{\partial H_{\mathrm{v}}}{\partial P}+\frac{r\rho_{\mathrm{w}}}{\rho_{\mathrm{w}}-\rho_{\mathrm{v}}}\left(\frac{\partial\rho_{\mathrm{v}}}{\partial P}\right)\right]V_{\mathrm{v}}+\left(\frac{\partial T_{\mathrm{t}}}{\partial P}c_{\mathrm{p\_t}}\right)X_{\mathrm{t}}} \tag{9a}$$

Under the conditions of Q_w=0 and $\Delta\dot{m}_f$=0, give the initial condition of the dynamic model, dP/dt=0. With the initial condition, Eq. (9a) can be transformed to,

$$\frac{\mathrm{d}P}{\mathrm{d}t}=\frac{Q_{\mathrm{w}}+(\varepsilon_1-H_{\mathrm{f}})\dot{m}_{\mathrm{f}}-\varepsilon_2\dot{m}_{\mathrm{v\_o}}}{\varepsilon_3V_{\mathrm{w}}+\varepsilon_4V_{\mathrm{v}}+\varepsilon_5X_{\mathrm{t}}} \tag{9b}$$

By comparison of Eqs. (9a) and (9b), it can be observe that ε_1, ε_2, ε_3, ε_4, and ε_5 can be easily acquired by the parameters of saturated water and steam, which are the function of pressure.

Condensation,

$$\dot{m}_{\mathrm{cond}}=\frac{b\dot{m}_{\mathrm{f}}(h_{\mathrm{w}}-h_{\mathrm{f}})}{h_{\mathrm{v}}-h_{\mathrm{w}}} \tag{10}$$

where, b represents the proportion of the steam generated by the steam in the evaporator when feed water enters. b is an empirical value which could be found from and 0.01 is chosen for b [32].

Evaporation,

$$\dot{m}_{\mathrm{evap}}=\frac{Q_{\mathrm{w}}-X_{\mathrm{w}}(h_{\mathrm{w}}-h_{\mathrm{w}})}{h_{\mathrm{v}}-h_{\mathrm{w}}} \tag{11}$$

$$\dot{m}_{\mathrm{d}}=\dot{m}_{\mathrm{evap}}P_{\mathrm{d}} \tag{12}$$

where P_{d} is the continuous discharging rate (%), P_{d}=2%.

$$\dot{m}_{\mathrm{vo}}=\xi\sqrt{P_{\mathrm{e}}-P_{\mathrm{s}}} \tag{13}$$

ξ is the admittance of the evaporator, which is depend on the characteristic of the valves. ξ=16.586.

The outside tube heat transfer coefficient can be expressed by,

$$U_o = \frac{Nu_o \times \lambda_w}{D_o} \tag{14}$$

$$Nu_o = 0.36\left[\frac{\dot{m}_{w\_max}\, D_o}{\mu_w}\right]^{0.35} Pr^{1/3} \tag{15}$$

The inner tube heat transfer coefficient,

$$U_i = \frac{Nu_i \times \lambda_s}{D_i} \tag{16}$$

$$Nu_i = 0.023 Re^{0.8} Pr^{1/3}\left[\frac{\mu_s}{\mu_{s\_wall}}\right]^{0.14} \tag{17}$$

(2) Superheater and preheater

The heat transfer fluid in the superheater and the preheater is a single phase. There is no phase change in both heat exchangers during the operation. Therefore they have the same mathematical model as follows. The differences are the phase of the working fluid and the range of the operating temperature.

The mass balance of steam/water,

$$V\frac{\mathrm{d}\rho_{\mathrm{v\_o}}}{\mathrm{d}t} = \dot{m}_{\mathrm{v\_i}} - \dot{m}_{\mathrm{v\_o}} \tag{18}$$

The energy balance of steam/water,

$$V\frac{\mathrm{d}\left(\rho_{\mathrm{v\_o}} h_{\mathrm{v\_o}}\right)}{\mathrm{d}t} = Q_{\mathrm{v}} + \dot{m}_{\mathrm{v\_i}} h_{\mathrm{v\_i}} - \dot{m}_{\mathrm{v\_o}} h_{\mathrm{v\_o}} \tag{19}$$

The heat transfer from tube bundle to steam/water,

$$Q_{\mathrm{v}} = A_{\mathrm{o}} U_{\mathrm{o}} \left(T_{\mathrm{t}} - T_{\mathrm{v}}\right) \tag{20}$$

The momentum balance of steam/water,

$$k_{\mathrm{d}}\frac{\dot{m}_{\mathrm{v\_i}}}{\rho_{\mathrm{v\_i}}} = P_{\mathrm{s\_i}} - P_{\mathrm{s}} \tag{20}$$

in which, k_d=2.911 in superheater, k_d=9.729 in preheater.

The energy balance at the tube bundle,

$$X_t c_{p\_t} \frac{dT_t}{dt} = Q_s - Q_v \tag{21}$$

The heat transfer from salt to the tube bundle,

$$Q_s = A_i U_i \left(T_s - T_t\right) \tag{22}$$

The energy balance on salt side,

$$\frac{d\left(c_{p\_s} M_s T_s\right)}{dt} = \dot{m}_s \left(h_{s\_i} - h_{s\_o}\right) - Q_s \tag{23}$$

3. Results and discussions

The simulation of the Solar Two steam generation system was carried out under the rated condition. The disturbance experiments were performed on the basis of rated condition. The inlet and outlet molten salt temperature of SGS are 565 °C and 288 °C, respectively. The feed water (265 °C, 10.00 MPa) enters SGS, and then the steam (535 °C, 9.00 MPa) flows out.

To get full acknowledgement of the dynamic characteristics of the SGS, five inlet parameters including valve opening, water mass flow rate, feed water temperature, molten salt temperature and molten salt flow rate step disturbance were imposed to SGS during operation under rated condition. The results indicate that the same increment and decrement of the same parameter has the opposite impact on the system output parameters, which means the curves with opposite trends could be achieved. The two kinds of response curves revealed the same dynamic characteristic. Thus, the increments and decrements were chosen at random in the following simulation.

3.1 Model validation

The designed operating parameters of Solar Two, as well as the calculated results, are illustrated in Table3. The validation test was carried out at rated condition of SGS. SGS thermal duty is 35.5 MW. Salt inlet temperature is 565 °C. Feed water temperature is 260 °C. Feed water inlet pressure is 10.0 MPa. The outlet parameters of molten salt and main steam are given by Table3. The results listed show that the difference between the data obtained by simulation and the designed values of Solar Two is very small, implying the validity of the present dynamic model.

Table 3. Comparisons between the simulation and the designed data of the objective SGS**.**

	Design value	Simulation value
Main steam pressure, MPa	9.00	9.00
Main steam temperature, °C	535.00	535.02
Pressure in evaporator, MPa	9.80	9.79
Evaporator outlet steam temperature, °C	310.00	309.51
Pressure in preheater, MPa	10.40	10.40
Molten salt outlet temperature,°C	288.00	287.99

3.2 Case study

During the operation of SGS, molten salt mass flow rate and temperature, as well as feed water mass flow rate and temperature were given as boundary conditions, they were also the main disturbance variables. Table 4 presents the boundary conditions of the simulation. Cases A-E could happen while a PT plant with TES operated as a peaking plant.

Table 4. Case definitions.

Index	Experiment	Inlet salt temperature(°C)	Molten salt flowrate(kg/s)	Feedwater temperature(°C)	Feedwater flow rate(kg/s)
A	Opening step of regulating valve of steam turbine at 100%-75% load	565	82.5	260	15.975
B	Water mass flow step at 100%-98%	565	82.5	260	15.656
C	Water inlet temperature step at 100% load	565	82.5	265	15.975
D	Molten salt inlet temperature step at 100% load	555	82.5	260	15.975
E	Molten salt mass flow step at 100%-95%	565	80.025; 79.2 ; 78.375	260	15.975

Case A

Fig. 2 illustrates the simulation results of case A defined in Table 3, including water side pressure, molten salt and water temperature. Operating under the rated condition, the opening of the regulated valve was turned down from 100% to 75% at 30 s. The rest of boundary conditions remained constant. For a self-regulating process, it can be observed that the outlet parameters of both fluid, molten salt and feed water, converged to their new steady state values finally. It took 420 s for the water side parameters to converge to their new steady state, as shown in Fig. 2(a), while it took about 400 s for salt side, which was shown in Fig. 2(b). When the steam quality decreased, more heat was absorbed by the steam per unit mass at first. Then it fell as the evaporation increased. This could be the reason that both the outlet steam temperature and outlet molten salt temperature of SGS decreased. It could also be the reason for that the sharp increasing of steam pressure in the evaporator and superheater, and then going down later, as shown in Fig. 2(c). The outlet mass flow rate of steam decreased to a certain level because the valve was turned down, then it increased as the self-control process works because the mass flow rate of molten salt did not change.

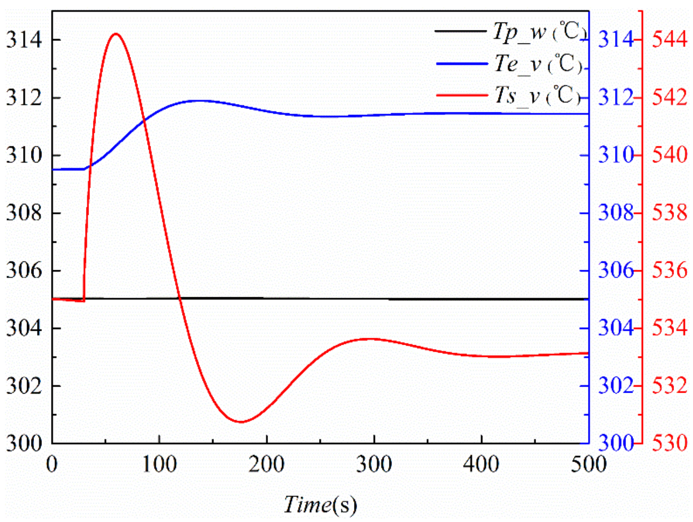

(a) Temperatures on the water side.

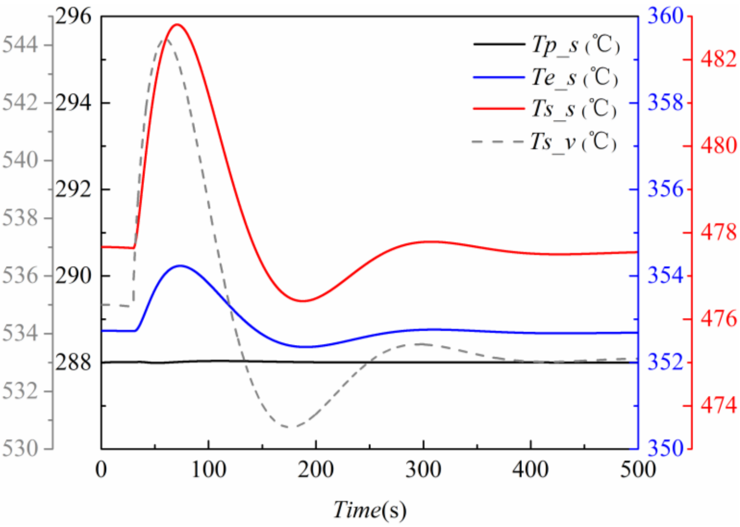

(b) Temperatures on the salt side.

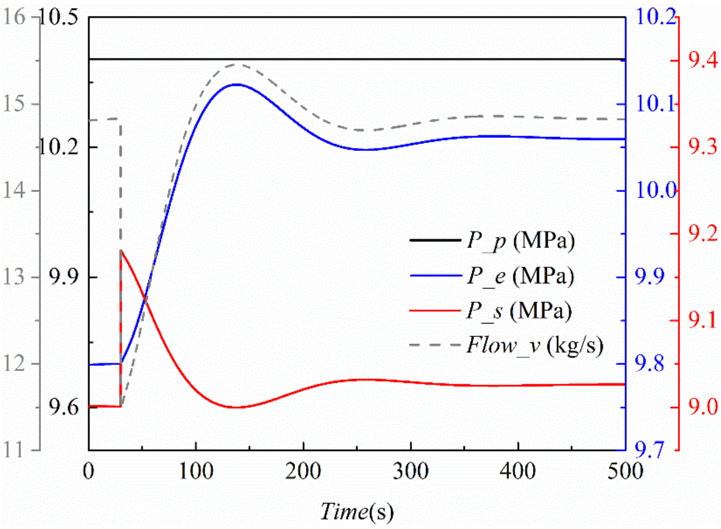

(c) Pressures on the water side.

Fig. 2. SGS parameters changes with valve opening decreased from 100% to 75% (case A).

The steady state was broken and 420 s later, a new steady state was reached. Molten salt is the shell side fluid in superheater, the large fluctuation of its temperature for short period could generate large thermal stress. Fortunately, large temperature fluctuations did not happen in the evaporator when SGS was operated under this condition. Otherwise, thermal stress would be larger for the shell of evaporator which should be designed to be thicker to sustain the high pressurized steam.

Unlike the steam temperature changes in the superheater, the steam temperature increased in the evaporator, which resulted from the redistribution of the heat load in the evaporator and superheater. Since the heat load increased and remain higher than it was in the evaporator, more water evaporated. In this case, the pressure in the evaporator increased and remain higher. But the molten salt outlet temperature did not change. As a result, the total heat load of SGS did not change even its distribution changed. Therefore, the flow rate of outlet steam decreased a little on condition that the evaporation increased.

Case B

The results of case B are shown in Fig. 3. Operating under the rated condition, the feedwater mass flow rate was subjected to a negative step disturbance at the beginning, changed from 15.975 kg/s to 15.775 kg/s. The rest of the boundary conditions remained constant. Because of a slight reduction of the feed water mass flow rate, the evaporation increased, the decrease of the steam outlet temperature and a slight increment of the molten salt outlet temperature were obtained. The temperature changes of the steam and molten salt in the evaporator took place in a minute and were less than 1 °C.

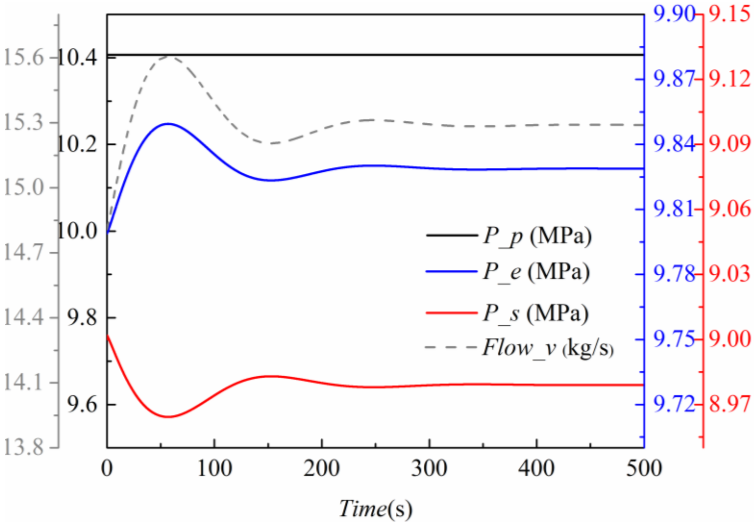

(a) Pressures on the water side

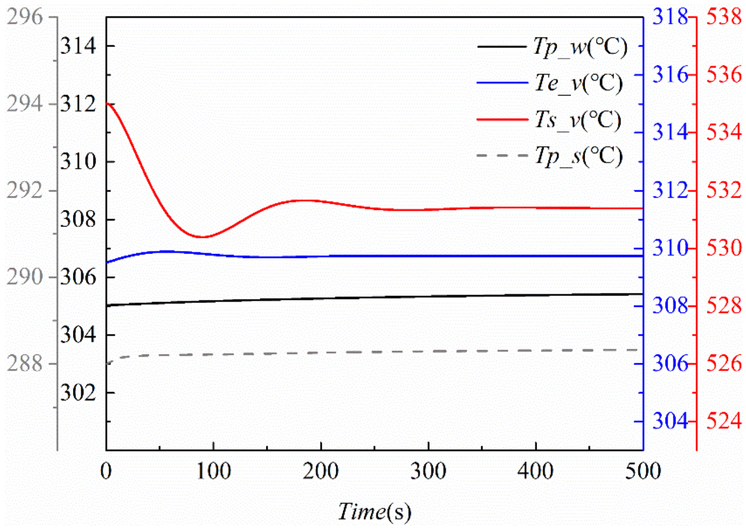

(b) Temperatures on the water side

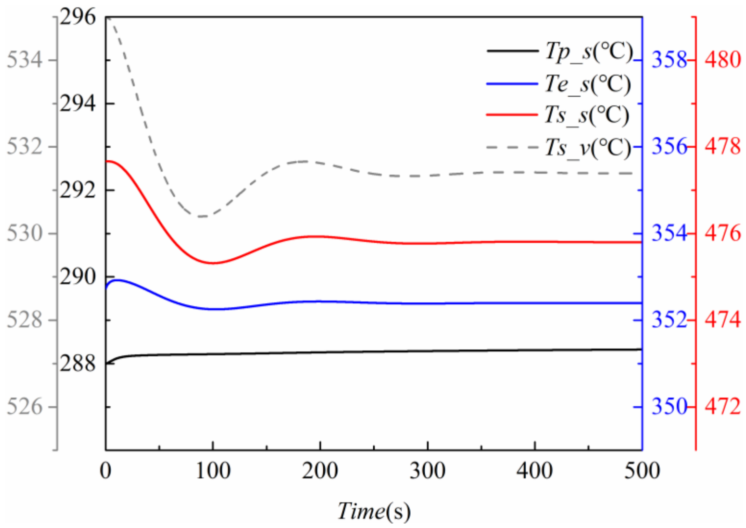

(c) Temperatures on the salt side

Fig. 3. SGS parameters changes with water mass flow rate decreased by 2% (case B)

Case C

Operating under the rated condition, the feed water inlet temperature was subjected to a positive step disturbance at the beginning, from 260 °C to 265 °C, and the results are shown in Fig.4. It can be found that the feedwater temperature step disturbance has insignificant impact on the system. Molten salt temperature rised swiftly to a value closed to the terminal in about 30 s. As the result, the steam outlet temperature needs 1200 s to reach to the steady state, but it took 1400 s for the feedwater temperature in the preheater. This is because water has higher specific thermal capacity and lower mass flow rate in contrast with steam. On the contrary, with lower specific thermal capacity and higher mass flow rate, molten salt responsed swiftly. Feedwater temperature has little influence on the outlet temperature of steam. The pressure changes were minute.

The results shown in Figs. 2-4 are acquired by imposing step disturbances to the water side. The parameters on salt side would response follow water side. Water mass flow rate has an obvious influence on the pressure of SGS. And it also leaded to the heat load reassignment to the evaporator and superheater. The direct influence of step disturbance of feed water temperature was the swift change of the molten salt outlet temperature. It should be noted that large temperature changes occured in the superheater when the step disturbances on water side were imposed to SGS, and pressure change of the steam in the evaporator and superheater were large.

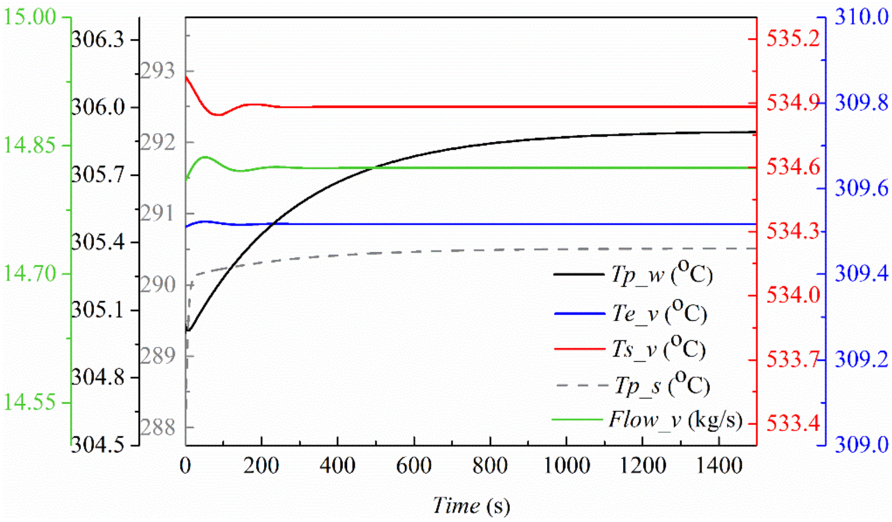

Fig. 4. Outlet temperature and pressure changes with feed water temperature increased by feed water 5 °C (case C)

Case D

As displayed in Fig. 5, the molten salt inlet temperature was subjected to a positive step change at the beginning, from 565°C to 575 °C. The other boundary conditions remained constant. The increase of the molten salt inlet temperature disorganized the heat distribution. As shown in Fig. 3, the quality of steam decreased, and the outlet steam temperature increased to adjust the heat load of superheater. The temperature change in superheater could be 14 °C. As a compraison, the evaporation change was small.

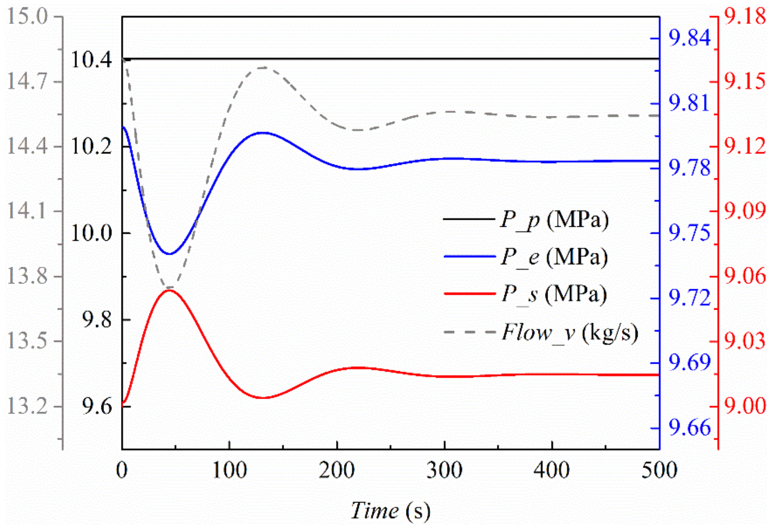

(a) Pressures on the water side

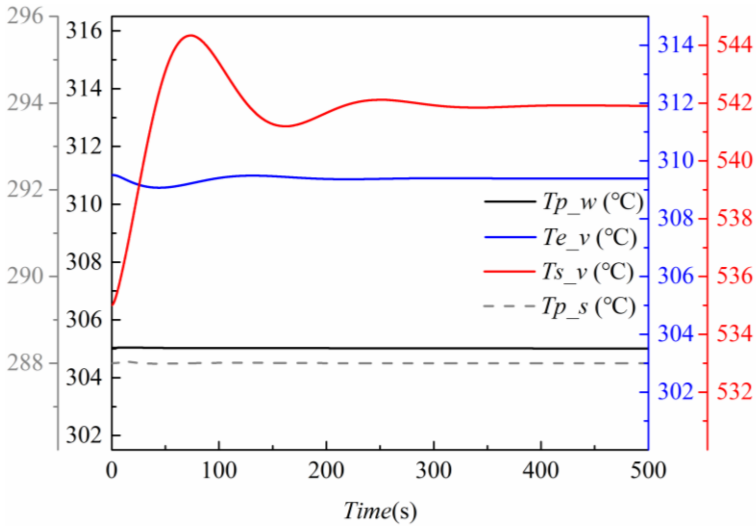

(b) Temperarures on the water side

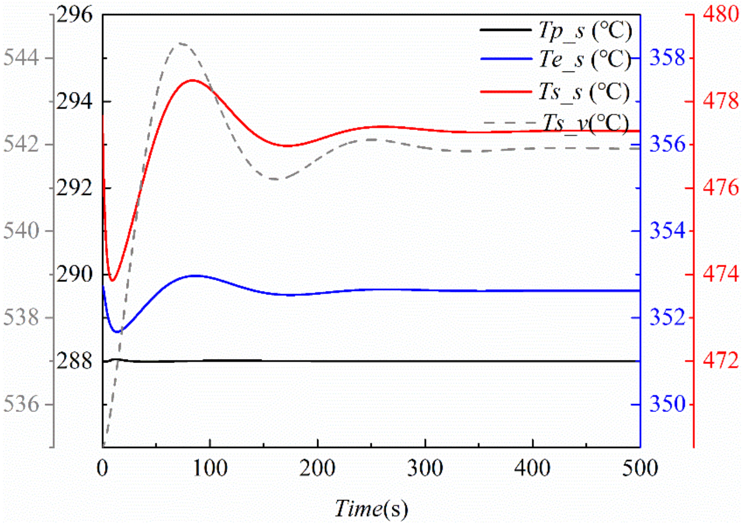

(c) Temperarures on the salt side

Fig. 5. SGS parameters changes with molten salt inlet temperature increased by 10 °C (case D)

Case E

For the unpredictability of solar irradiance, it is difficult to control the temperature of the heat transfer fluid. To make sure the stability of the solar power tower operation, the goal of the control strategies is to control the mass flow rate of the HTF (heat transfer fluid) to stabilize the molten salt outlet temperature. Since the variation of the solar irradiance is large, the variation of the molten salt mass flow rate is large as well. Therefore, the dynamic characteristic of the heat transfer feedback is obvious, such as response time and delay [18]. A detailed study for the purpose noted above (case E) was performed. The step-by-step disturbance of the molten salt mass flow rate was imposed to the system under the rated condition. The results are displayed in Fig. 6 and 7.

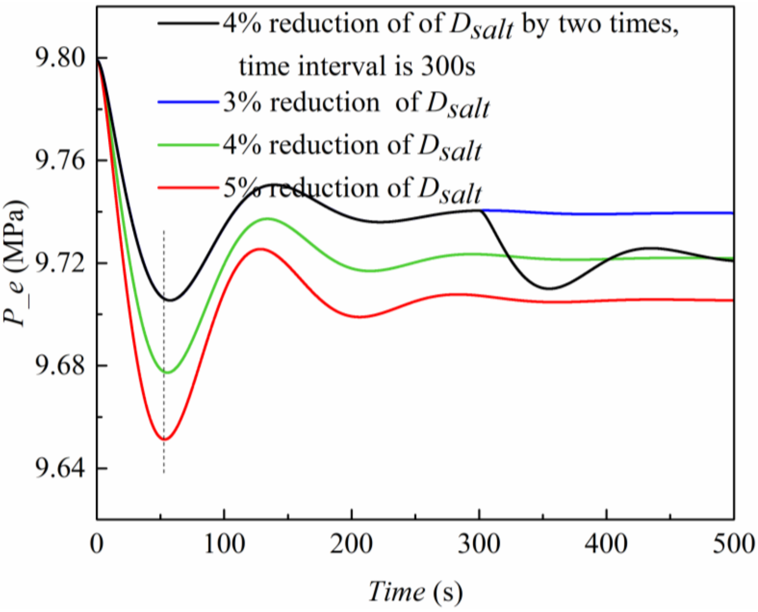

(a) Evaporator pressures on the water side

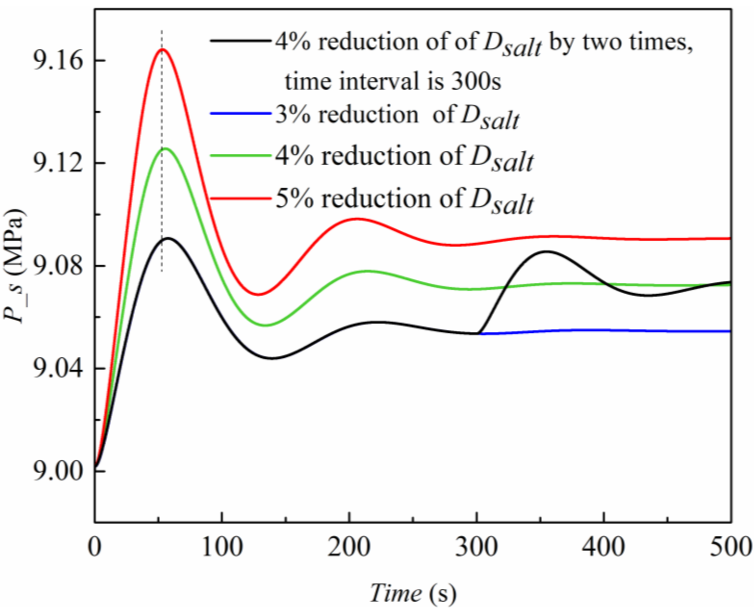

(b) Superheater pressures on the water side

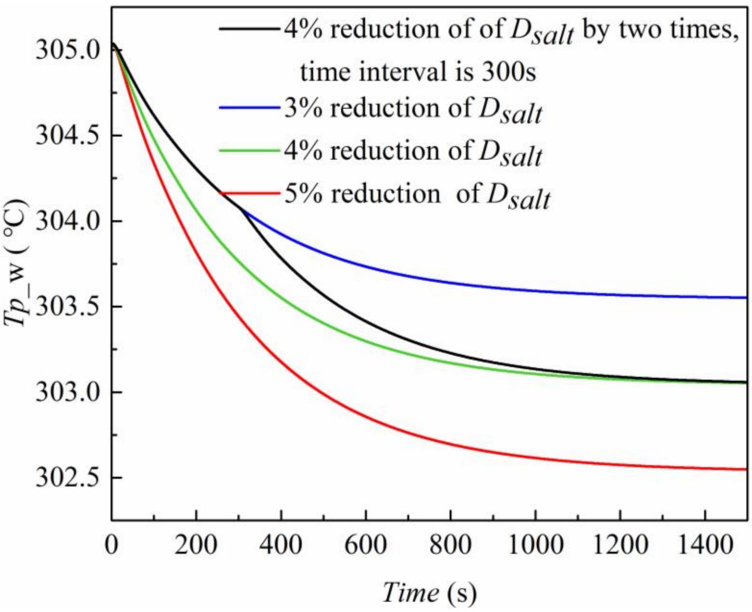

(c) Temperatures of water in the preheater

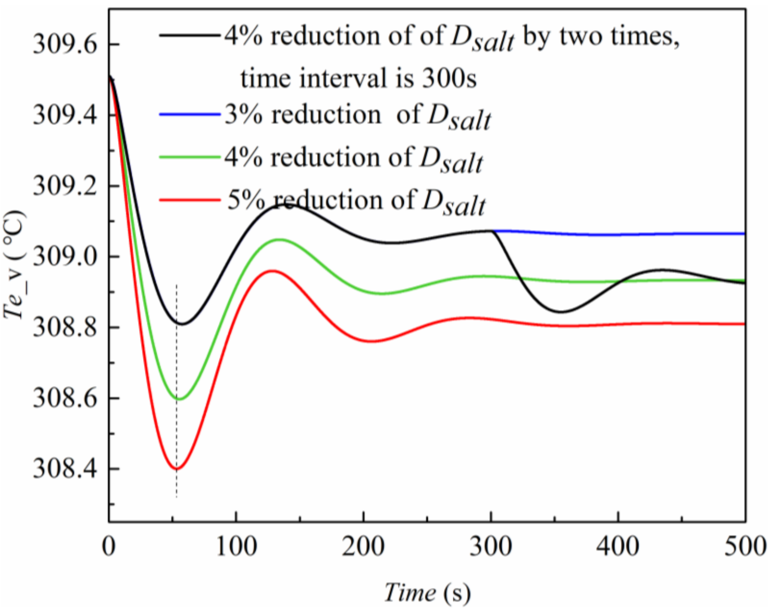

(d) Temperatures of steam in the evaporator

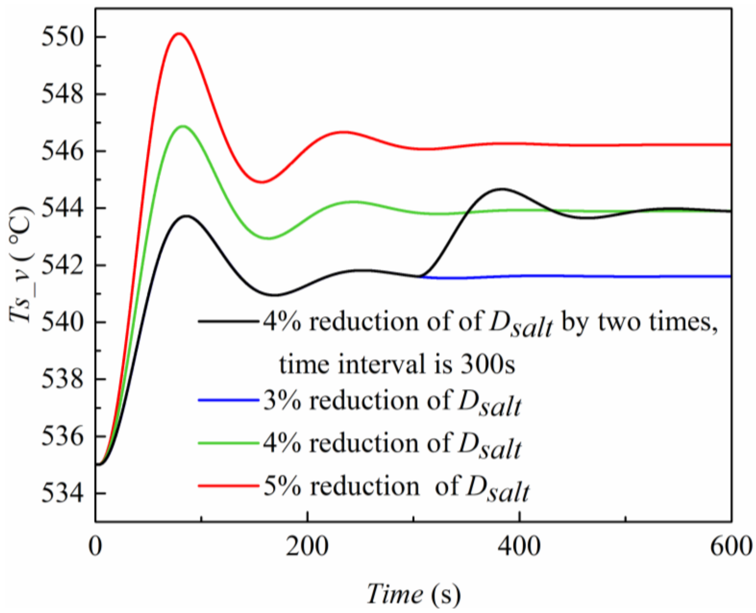

(e) Temperatures of steam in the superheater

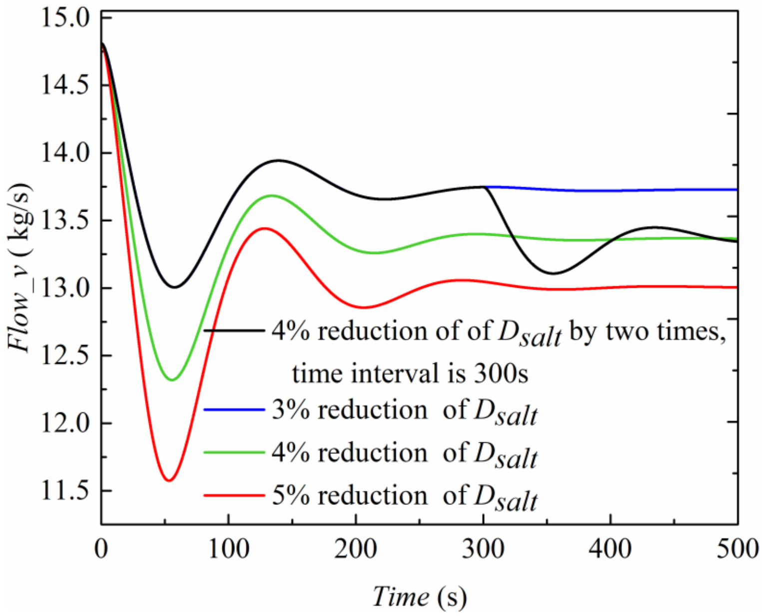

(f) Flow rate of steam

Fig. 6. SGS parameters changes with molten salt mass flow rate decreased by 3-5% (case E)

At the beginning, the molten salt mass flow rate changed from 100% load to 97%, 96%, and 95% load, respectively, with the rest of the boundary conditions remained constant. In principle, the outlet temperature responses experienced the same transients change as shown in Fig. 6 and Fig. 7. The time constants on water side of the three heat exchangers are 400 s, 420 s, and 1400 s, respectively, whereas on salt side, the time constants are 380 s, 400 s, and 1200 s, respectively. The preheater has the largest thermal capacity, and while the superheater has the smallest. This is because the specific thermal capacity of water is much bigger than that of steam.

As demonstrated in Figs. 6 and 7, the time is shorter as molten salt mass flow rate decreased, which the parameters of steam and molten salt needed to reach to their extremum and recover to their steady state before they reach to the new steady state. But the time difference of time constant under different step disturbance of mass flow rate is short. The step disturbance is the driving impetus of changes of the system working condition. When it is smaller, the longer SGS needs to reach to its extremum.

When the mass flow rate of molten salt decreased, SGS outlet temperature increased. This can be explained by the fact that the decrease of the heat transfer to water side leaded to the reduction of evaporation. On the contrary, the steam temperature in the evaporator decreased for the heat provided was less than before. The molten salt outlet temperature increment could as big as 16 °C which attention should be paid when PT is operated under similar load variations.

During the operation under the rated condition, step-by-step disturbance of molten salt mass flow rate was imposed to the system. Mass flow rate dropped from 100% load to 96% load. Boundary conditions and disturbances were same to the former simulation, but the reduction was divided into two steps. At initial stage, the mass flow rate decreased from 100% load to 97% load, then it decreased to 96% load at 300 s which closed to the steady state of the system (the time difference was chosen on the basis of the time of the large fluctuation of the temperatures). The response curves are the black lines shown in Figs. 6 and 7. The black lines and the green lines converge to the same values when the system reached to a steady state. But they differ from the green lines with lowering the fluctuations notably. By using SDM, the reductions of the parameter fluctuations are 0.2 °C (steam outlet temperature in the evaporator), 1.5 °C (steam outlet temperature in the superheater), 0.03MPa (steam outlet pressure), 0.7 °C (molten salt outlet temperature in the evaporator), and 1 °C (molten salt outlet temperature in the superheater).

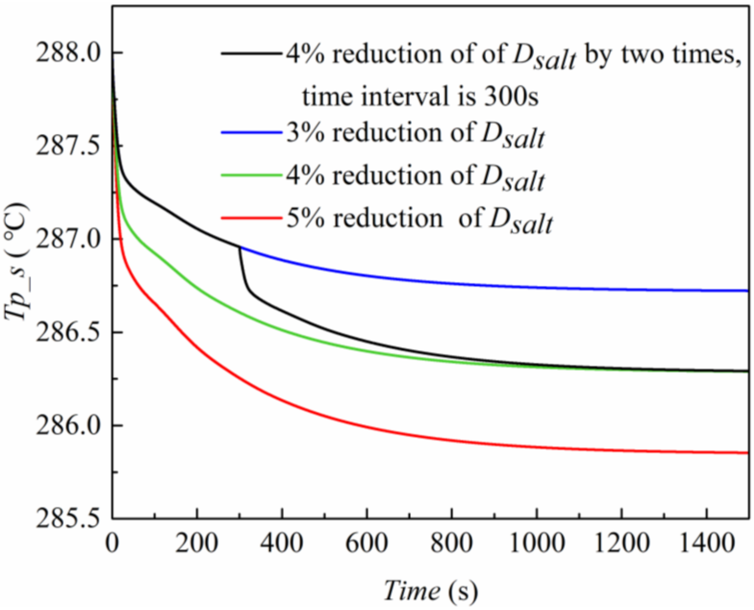

(a) Temperatures of salt in the preheater

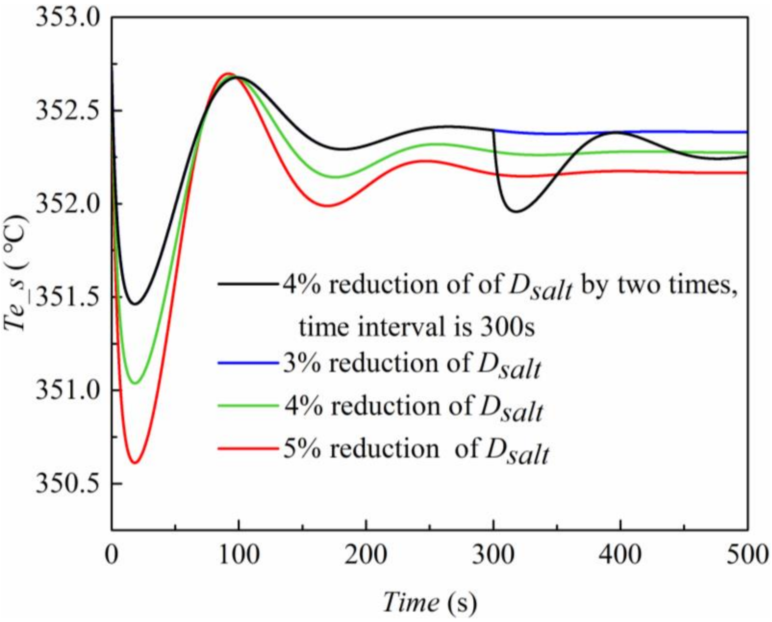

(b) Temperatures of salt in the evaporator

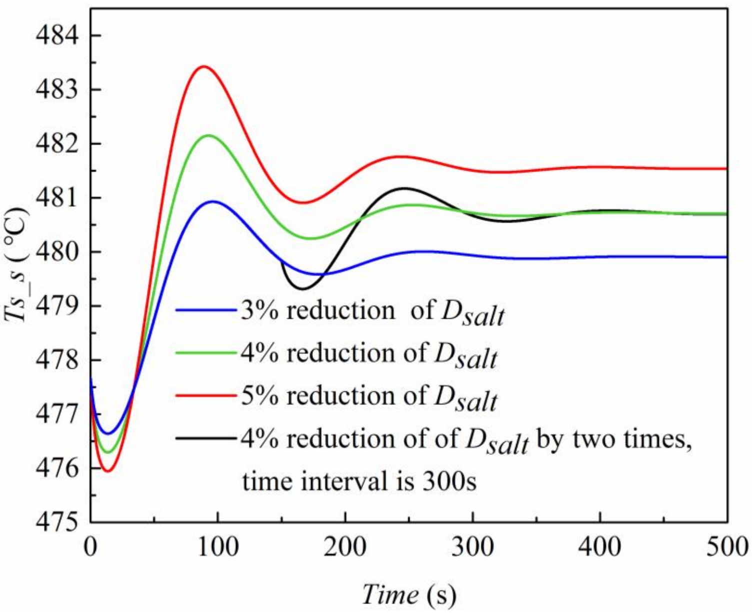

(c) Temperatures of salt in the superheater

Fig. 7. Molten salt temperature changes in the preheater with molten salt mass flow rate decreased by 3-5% (case E)

4. Conclusions

The mathematical model with LPM is built to analyze the dynamic characteristic of the steam generation system (SGS) in solar tower power plant after the static validation. Five simulation tests were carried out considering the disturbances that the solar tower power plant may encounter during the variable load conditions. Case A, B, C could occur for both molten salt PT and traditional plants, whereas Case D, E could only occur to this kind of solar system. Because of the differences of the heating source and control strategies between this kind of solar system and traditional power plant, temperature and flow rate will not change separately in a traditional power plant. The following conclusions can be achieved.

(1) The disturbances imposed to the working fluids lead to the heat load reassignment to the preheater, evaporator and superheater.

(2) Large temperature and pressure fluctuations in the superheater, including the outlet steam temperature, steam pressure and outlet molten salt temperature are caused by the disturbances, especially the change of molten salt flow rate. These changes during short period are the causes for large thermal stress which will reduce the service life of the superheater.

(3) The thermal capacity of the heat exchangers or the thermal inertia of SGS has been displayed. The preheater has the biggest thermal capacity while the superheater has the smallest. The time constants of the three heat exchangers have been acquired, which are good references for the test of various operating control strategies.

(4) The proposed SDM on the basis of time constant can reduce the fluctuation of the outlet fluid parameters. Working conditions have influence on the time constants. This provides an example for the control strategies to reduce the temperature and pressure fluctuations, including the decision making of the minimum stable load and net load ramp rate.

(5) Five disturbance experiments was conducted. The variation trends of steam temperature, steam pressure, and steam flow were obtained and discussed. The results obtained could be the good references for the design and operation of solar thermal power tower system.

Acknowledgements

The financial supports from the National Natural Science Foundation of China (No. 51676069), the State Grid Science and Technology Program of China (No. GTLN201706-KJXM001) and the Royal Academy of Engineering of UK (DVF1718\8\26) are gratefully acknowledged.

References

[1] Wang N. Large-Scale Wind Power Grid Integration, in: Introduction; E-Publishing Inc., Oxford,pp 2016. 3-17.

[2] Hong W Y, Jin H D. China's energy storage industry: Develop status, existing problems and countermeasures. China Energy Storage Alliance.Renewable and Sustainable Energy Reviews 2016; 71, 767-784.

[3] Li C, Shi H, Cao Y. Comprehensive review of renewable energy curtailment and avoidance: A specific example in China. Renewable& Sustainable Energy Reviews 2015.41, 1067-1079.

[4] Eyer J M, Corey G P. Energy storage for the electricity grid : benefits and market potential assessment guide: a study for the DOE Energy Storage Systems Program. Geburtshilfe Und Frauenheilkunde 2010; 45(5):322-5.

[5] Barde A, Jin K, Shinn M. Demonstration of a low cost, high temperature elemental sulfur

thermal battery. Applied Thermal Engineering 2018. 137, 259-267.

[6] Kim D H, Yoon S H, Kim Y. Experimental studies of the discharge performance of single-medium TES for CSP applications. Applied Thermal Engineering 2017. 127, 499-507.

[7] Wood D L, Li J, Daniel C. Prospects for reducing the processing cost of lithium ion batteries. Journal of Power Sources 2015. 275, 234-242.

[8] Li X, Xu E, Song S. Dynamic simulation of two-tank indirect thermal energy storage system with molten salt. Renewable Energy 2017. 113, 1311-1319.

[9] Herrmann U, Kelly B, Price H. Two-tank molten salt storage for parabolic trough solar power plants. Energy 2004. 29(5), 883-893.

[10] Zhou X, Xu Y. Solar updraft tower power generation. Solar Energy 2016. 128, 95-125.

[11] Mark Mehos C. T, J. V. Concentrating Solar Power Gen3 Demonstration Roadmap. National Renewable Energy Laboratory Technical Report 2017.

[12] Flesch R, Frantz C, Maldonado Quinto D. Towards an optimal aiming for molten salt power towers. Solar Energy 2017. 155, 1273-1281.

[13] Denholm P, Mehos M. Enabling Greater Penetration of Solar Power via the Use of CSP with Thermal Energy Storage. Office of Scientific & Technical Information Technical Reports 2011.

[14] Mertens N, Alobaid F, Frigge L. Dynamic simulation of integrated rock-bed thermocline storage for concentrated solar power[J]. Solar Energy 2014. 110, 830-842.

[15] Augspurger M, Udaykumar H S. Transient multi-day simulations of thermal storage and heat extraction for a finned solar thermal storage device. Solar Energy 2017. 151, 48-60.

[16] Ampuño G, Roca L, Berenguel M. Modeling and simulation of a solar field based on flat-plate

collectors. Solar Energy 2018. 170, 369-378.

[17] Shah L J, Morrison G L, Behnia M. Characteristics of Vertical Mantle Heat Exchangers For Solar Water Heaters. Solar Energy 1999, 67(1), 79-91.

[18] González-Gómez P A, Gómez-Hernández J, Briongos J V. Thermo-economic optimization of molten salt steam generators. Energy Conversion & Management 2017. 146, 228-243.

[19] Ruiz-Cabañas F J, Prieto C, Jové A. Steam-PCM heat exchanger design and materials optimization by using Cr-Mo alloys. Solar Energy Materialsand Solar Cells 2018. 178,249-258.

[20] TEMA. Tubular Exchanger Manufacturers Association Standards 2007.

[21] Wu J, Hou H, Hu E. Performance improvement of coal-fired power generation system integrating solar to preheat feedwater and reheated steam[J]. Solar Energy 2018. 163, 461-470.

[22] Skoglund T, Årzén K, Dejmek P. Dynamic object-oriented heat exchanger models for simulation of fluid property transitions. International Journal of Heat and Mass Transfer 2006.

[23] Zaversky F, Sánchez M, Astrain D. Object-oriented modeling for the transient response simulation of multi-pass shell-and-tube heat exchangers as applied in active indirect thermal energy storage systems for concentrated solar power. Energy 2014. 65, 647-664.

[24] Rees S. J. An extended two-dimensional borehole heat exchanger model for simulation of short and medium timescale thermal response. Renewable Energy 2015. 83, 518-526.

[25] Zhang J, He Y, Tao W. 3D numerical simulation on shell-and-tube heat exchangers with middle-overlapped helical baffles and continuous baffles– Part I: Numerical model and results of whole heat exchanger with middle-overlapped helical baffles. International Journalof HeatAnd Mass Transfer 2009. 52(23), 5371-5380.

[26] Ozden E, Tari I. Shell side CFD analysis of a small shell-and-tube heat exchanger. Energy Conversion and Management 2010. 51(5), 1004-1014.

[27] You Y, Fan A, Huang S, 2012. Numerical modeling and experimental validation of heat transfer and flow resistance on the shell side of a shell-and-tube heat exchanger with flower baffles. International Journal of Heat and Mass Transfer. 55(25), 7561-7569.

[28] Xu E, Yu Q, Wang Z, et al. Modeling and simulation of 1 MW DAHAN solar thermal power tower plant. Renewable Energy 2011, 36(2):848-857.

[29]Xu E, Wang Z, Wei G, et al. Dynamic simulation of thermal energy storage system of Badaling 1MW solar power tower plant. Renewable Energy 2012; 39(1):455-462.

[30] Zavoico A. B. Solar Power Tower Design Basis Document. Office of Scientific & Technical Information Technical Reports 2001.

[31] Stokes J W, Holly L, Mayer K H. The ASME boiler and pressure vessel code. Non-Destructive Testing 1974. 7(3), 145-151.

[32] Zhang Ch. Dynamic characteristics and model of boiler. Water Resources and Electric Power Press, 1987

Table captions

Table 1. Geometrical and physical parameters of SGS.

Table 2. The physical properties of the molten salt.

Table 3. Comparisons between the simulation and the designed data of the objective SGS**.**

Table 4. Case definitions.

Figure captions

Fig. 1. The schemeticdiagram of SGS**.**

Fig. 2. SGS parameters changes with valve opening decrease from 100% to 75% (case A). (a) Temperatures on the water side. (b) Temperatures on the salt side. (c) Pressure on the water side.

Fig. 3. SGS parameters changes with water massflow rate decreases by 2% (case B). (a) Pressures on the water side. (b) Temperatures on the water side. (c) Temperatures on the salt side.

Fig. 4. Outlet temperature and pressure changes with feed water temperature increases by feed water 5°C (case C).

Fig. 5. SGS parameters changes with molten saltinlet temperature increased by 10°C (case D). (a) Pressures on the water side. (b) Temperatures on the water side. (c) Temperatures on the salt side.

Fig. 6. SGS parameters changes with molten salt mass flow rate decreased by 3-5% (case E). (a) Evaporator pressures on the water side. (b) Superheater pressures on the water side. (c) Temperatures of molten salt in the preheater. (d) Temperatures of steam in the evaporator. (e) Temperatures of steam in the superheater. (f) Flow rate of steam.

Fig. 7. Molten salt temperature changes in the preheater with molten salt mass flow rate decreased by 3-5% (case E). (a) Temperatures of salt in the preheater. (b) Temperatures of salt in the evaporator. (c) Temperatures of salt in the superheater.